Uykan, Zekeriya; Al-Tous, Hanan; Yiğitler, Hüseyin; Jäntti, Riku; Tirkkonen, Olav

Angle-Delay Features and Distances for Channel Charting

Published in:
2024 IEEE Wireless Communications and Networking Conference, WCNC 2024 - Proceedings

DOI:
10.1109/WCNC57260.2024.10571176

Published: 01/01/2024

Document Version
Peer-reviewed accepted author manuscript, also known as Final accepted manuscript or Post-print

Angle-Delay Features and Distances for Channel Charting

Zekeriya Uykan[1], Hanan Al-Tous[2], Hüseyin Yiğitler[2], Riku Jäntti[2], and Olav Tirkkonen[2]

[1]College of Engineering and Technology, American University of the Middle East, Kuwait
[2]Department of Information and Communications Engineering, Aalto University, Finland
Email: zekeriya.uykan@aum.edu.kw, {hanan.al-tous, huseyin.yigitler, riku.jantti, olav.tirkkonen}@aalto.fi,

***Abstract*—Channel charting (CC) is an unsupervised machine learning framework for learning a lower-dimensional representation of Channel State Information (CSI), while preserving spatial relations between CSI samples. In this paper, we consider super-resolution features in the angle-delay domain in massive Multiple-Input Multiple-Output (MIMO) systems. We *i)* treat the angle and delay separately, *ii)* present the so-called "Normalized Polar Feature" utilizing the channel statistics of the CSI samples, *iii)* use the Euclidean distance to compute the dissimilarity matrix, and create the channel chart. Simulation results based on the DeepMIMO data-set show that the proposed super-resolution representation with the Euclidean distance leads to the state-of-the-art quality CC as compared to other CSI features and distances from the literature such as angle-delay-power features with earth mover distance.**

***Index Terms*—Channel charting, channel state information, multi-path components, super-resolution feature, feature distance.**

I. Introduction

Beyond fifth-Generation mobile communication systems have several enablers such as massive Multiple-Input Multiple-Output (MIMO) techonology, beamforming, huge amounts of available spectrum, small cell networks to achieve sub-meter positioning accuracy, and embedded sensing capabilities [1], [2].

Radio resource managements increasingly rely on knowledge about the geographical location of the User Equipments (UEs) to support high-level network functions, such as handover between base stations and beam management. Existing positioning approaches require a significant amount of dedicated resources to obtain feedback from the UE. They are also not universally applicable: UEs may not have Global Navigation Satellite System (GNSS) positioning capabilities, they may be indoors or without satellite coverage [1], [3]. For many radio resource management applications, absolute position information is not required: a pseudo-location that accurately represents neighborhood relationships may be sufficient.

Channel Charting (CC) has recently emerged as a framework for relative localization [4]. CC consists of learning a mapping between Channel Sate Information (CSI) samples and points in a so-called channel chart. This mapping is constructed such that nearness between two points on the channel chart indicates similarity between the corresponding CSI samples, their propagation conditions. Conventional dimensionallity reduction techniques such as Laplacian Eigenmaps, Sammon's mapping, Isomap and t-Distributed Stochastic Neighbor Embedding (t-SNE) can be used to construct the chart [5]. These techniques rely on a matrix of pair-wise distances between any two CSI features. Several linear algebraic distances, such as Euclidean, cosine similarity, correlation matrix distance, and log-Euclidean distance, are used to measure the distance between CSI features [4], [6], [7]. CC can be also constructed from the CSI features directly without invoking a feature distance using auto-encoder or from triplet Nural Networks with some side information [4], [8].

Channel modeling studies have demonstrated that the wireless channel can be characterized by a set of few parameters, such as angle of arrival, angle of departures and delays of multipath components [9], [10]. Capitalizing on this, the super-resolution angle-delay-power profile is considered for CC in [11]. The super-resolution feature is represented as a point in the 2D Cartesian coordinate system. The Earth-Mover Distance (EMD) is used to measure the feature distance. Simulation results show that the super-resolution features with EMD outperform other features and distances in terms of local topology preservation and global geometry preservation performance measures [11].

In this paper, we consider super resolution features as in [11]. However, we *i)* treat the angle and delay separately (not as 2D Cartesian coordinates), *ii)* present the *Normalized Polar Feature* utilizing delay and angle of arrival statistics of multi-path components, *iii)* use the Euclidean distance to measure the distance between normalized polar features, which is of much reduced computational complexity compared to EMD, *iv)* investigate several CSI feature representations with the Euclidean distance, *v)* combine the distances of several feature representations, *vi)* evaluate different features performance in terms of local topology preservation and global geometry preservation measures, and *vii)* create the channel chart.

The remainder of this paper is organized as follows: In Section II, the system model is presented. In Section III, CSI features and distances from literature are presented. In Section IV, the proposed super-resolution CSI features and distances are introduced. In Section V, channel charting is discussed. In Section VI, the performance measures are presented. Simulation results are presented and discussed in Section VII. Finally, conclusions are drawn in Section VIII.

II. System Model

We consider a massive MIMO Base Station (BS) with a Uniform Linear Array (ULA) of M antennas. The wireless signal transmitted from a UE propagates along K multipaths. The baseband channel response vector at the BS form multipath component k arising from an impulse transmitted at time 0 is

$$\mathbf{c}_k = \sqrt{\alpha_k} e^{-j\beta_k} \mathbf{a}(\theta_k)\, \delta(\tau_k), \tag{1}$$

where $\delta(\cdot)$ is the Dirac delta distribution, $\sqrt{\alpha_k} e^{-j\beta_k}$ is the complex attenuation, τ_k the propagation delay, and θ_k the Angle-of-Arrival (AoA) of path k. The array steering vector corresponding to AoA θ is

$$\mathbf{a}(\theta) = [1, e^{-j2\pi \frac{r \sin\theta_k}{\lambda_c}}, \ldots, e^{-j2\pi \frac{r(M-1)\sin\theta_k}{\lambda_c}}]^{\mathrm{T}}, \tag{2}$$

where r is the antenna element spacing, and λ_c is the carrier wavelength.

Considering an Orthogonal Frequency-Division Multiplexing (OFDM) system with N subcarriers, assuming the cyclic prefix is larger than the maximum delay spread, the channel frequency response vector at the nth subcarrier becomes

$$\mathbf{h}_n = \sum_{k=0}^{K-1} \sqrt{\alpha_k} e^{-j\beta_k} \mathbf{a}(\theta_k)\, e^{-j2\pi n \frac{\upsilon_k}{N}}, \tag{3}$$

where $\upsilon_k = \lfloor \frac{\tau_k}{T} \rceil$ denotes the temporally resolvable propagation delay associated with the kth path, T is the sample interval, and $\lfloor\, \rceil$ is rounding to the next integer.

III. CSI Features and Distances

For fingerprinting based localization and CC, several CSI features have been considered such as CSI frequency response, covariance matrix and super resolution features [4], [12]–[14]. The selection of the CSI feature as well as the feature distance highly affects the resulting performance.

A. Super Resolution Features

Assume that the channel has K multipath components (MPCs), represented by angle of arrivals θ_k, propagation delays τ_k and average powers p_k with $p_k = \mathbb{E}\{\alpha_k\}$ for $k = 1, \ldots, K$. Here, $\mathbb{E}\{\cdot\}$ denotes expectation. The angle-delay-power profile $\{\phi_k,\, \tau_k,\, p_k\}$ is the super-resolution CSI feature, which can be estimated from the channel frequency response using the Mutiple Signal Classification (MUSIC) and the Space-Alternating Generalized Expectation-Maximization (SAGE) algorithms [10], [15]. Several super resolution CSI representations are considered for CC and for multi-path component clustering [11], [16]–[18]. We summarize the super resolution representations from the literature as follows:

- The Multi-Path Separation (MPS) feature of multipath component k of UE i is [17], [18]

$$\mathbf{f}^{i,k}_{\mathrm{MPS}} = \begin{bmatrix} \cos(\theta_{i,k}) \\ \sin(\theta_{i,k}) \\ \zeta\, \tau_{i,k}/\tau_{\max} \end{bmatrix}, \tag{4}$$

  where $\theta_{i,k}$, and $\tau_{i,k}$ are the AoA and delay of MPC k of UE i, $\tau_{\max}$ is the maximum delay and ζ is a weight.

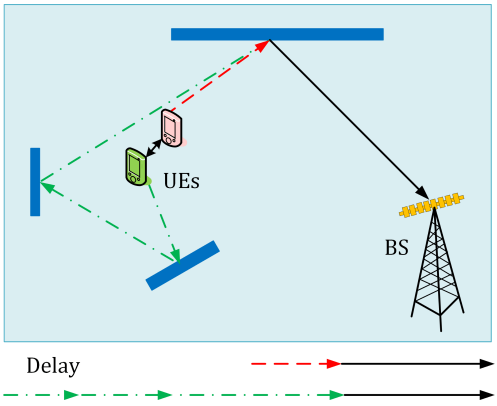

Fig. 1. Two nearby UEs; the received signals at the BS are with the same angle, but with but with large delay difference.

- The Angle-Power Feature (APF) is given as [16]:

$$\mathbf{f}^{i,k}_{\mathrm{APF}} = \begin{bmatrix} p_{i,k}^{-1/\nu} \cos(\theta_{i,k}) \\ p_{i,k}^{-1/\nu} \sin(\theta_{i,k}) \end{bmatrix}, \tag{5}$$

  where $p_{i,k}$ is the power of MPC k of UE i and ν is the path-loss exponent.
- The Super-resolution Rectangular Feature (SRF) is given as [11]:[1]

$$\mathbf{f}^{i,k}_{\mathrm{SRF}} = \begin{bmatrix} \tau_{i,k} \cos(\theta_{i,k}) \\ \tau_{i,k} \sin(\theta_{i,k}) \end{bmatrix}. \tag{6}$$

B. Super Resolution Distances

It is not straightforward to measure the distance between two super-resolution CSI features. Different orderings of the MPCs may result in different distances, and handling two features with different number of MPCs is not trivial. In [11], the powers of MPCs are converted to normalized weights and EMD is used to compute the distance between two sets of MPCs, to obtain the distance a linear programming is solved.

IV. Normalized Polar Feature and Distance

The super rectangular feature maps the angle and delay of a MPC to 2D point in the space. This model couples the delay and AoA, i.e., a nearby point needs to have a small change in both the AoA and delay. Figure 1 illustrates a scenario of two UEs transmitting from nearby physical locations. The received signal at the BS from each UE has one MPC. The propagation delay of the green UE is much larger than the propagation delay of the red UE, as shown by the length of green dashed line compared to length of red dashed line. There is no angular difference between the received signals from the two UEs at the BS. If the super rectangular features of the two UEs are used with the Euclidean distance, a large distance is obtained. To handle such challenging scenarios, we treat the angle and delay separately. We consider the "Normalized Polar Feature (NPF)" expressed as:

$$\mathbf{f}^{i,k}_{\mathrm{NPF}} = \begin{bmatrix} \theta_{i,k}/a_\theta \\ \tau_{i,k}/a_\tau \end{bmatrix}, \tag{7}$$

[1]Also known as the 2D Cartesian coordinate super resolution feature.

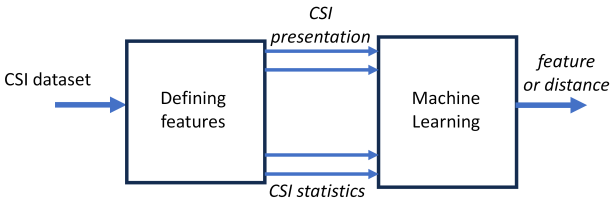

Fig. 2. The problem of determining optimum feature vectors and distance matrix for CC using machine learning.

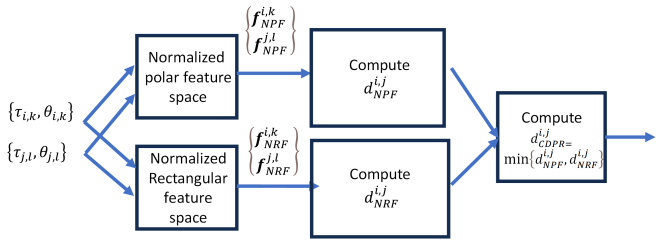

Fig. 3. The combining method to calculate the distance (dissimilarity) between two UEs using two CSI features / distances.

where the normalization factors $a_\theta = \max_{i,k} \theta_{i,k}$, and $a_\tau = \max_{i,k} \tau_{i,k}$. The normalization factors are proposed to handle different scales of the AoA and delay.

To compute the distance between two normalized features $\mathbf{f}^{i,k}_{\text{NPF}}$ and $\mathbf{f}^{j,l}_{\text{NPF}}$ between MPC k of UE i and MPC l of UE j, we use the Euclidean distance, i.e.,

$$d\left(\mathbf{f}^{i,k}_{\text{NPF}}, \mathbf{f}^{j,l}_{\text{NPF}}\right) = \|\mathbf{f}^{i,k}_{\text{NPF}} - \mathbf{f}^{j,l}_{\text{NPF}}\|_2.$$

To compute the CSI distance between UE i having K MPCs and UE j having L MPCs, we consider the minimum pair-wise distances, i.e.,

$$d^{i,j}_{\text{NPF}} = \min_{k,l} d\left(\mathbf{f}^{i,k}_{\text{NPF}}, \mathbf{f}^{j,l}_{\text{NPF}}\right), \tag{8}$$

where $k = 1, \ldots, K$ and $l = 1, \ldots, L$.

A. Feature and/or Distance Selection

The optimum feature formation depends on the CSI data characteristics like Line-of-Sight (LoS), Non-Line-of-Sight (NLoS), the CSI statistics (angle spread,...), etc.

The normalized polar feature may provide better results in challenging NLoS scenarios, whereas the rectangular feature may provide better results when the signals from nearby UEs propagate through similar paths. The CC quality depends on the feature representation as well as the distance chosen. There is not a unique feature vector formation and distance which gives the best CC performance for any wireless environment.

In this paper, we post the following "optimum feature and/or distance selection problem using Machine Learning (ML)" as a future research direction. We formulate it as follows: Given a specific CSI dataset representing a unique wireless environment and a set of feature vectors like the SRF, MPS, APF and NPF presented on the previous subsections and among others, how can we find the optimum feature vectors with optimum weights and optimum distance matrix to yield a good CC or accurate fingerprint localization? This optimization problem is depicted in Figure 2. Because solving the "optimum feature vector selection problem by ML" is out of the scope of this paper, in what follows we propose a novel simple method to combine different distances (dissimilarities) for CC.

B. CDPR: Combining Distances of the Normalized Polar and Rectangular Features

As illustrated by Figure 1 where there is no angular difference and the difference between propagation delays is large, it is expected that the normalized polar feature performs better since only its delay component has a large deviation, whereas for the rectangular feature, both component have large deviation. On the other hand, when LoS propagation exists between UE and BS, the rectangular feature is expected to perform better. Correspondingly, selecting the feature that yields smaller distance is a natural choice for combining these features. We summarize our method as "Combining distances from two features/distances by *minimum* operation". The combining method can be used with any two features/ distances. Figure 3 explains the combining idea using two features / distances.

We propose the "Normalized Rectangular Feature (NRF)" expressed as:

$$\mathbf{f}^{i,k}_{\text{NRF}} = \begin{bmatrix} \tau_{i,k} \cos\left(\theta_{i,k}\right) / a_{\text{c}} \\ \tau_{i,k} \sin\left(\theta_{i,k}\right) / a_{\text{s}} \end{bmatrix}, \tag{9}$$

where $a_{\text{c}} = \max_{i,k} |\tau_{i,k} \cos\left(\theta_{i,k}\right)|$, and $a_{\text{s}} = \max_{i,k} |\tau_{i,k} \sin\left(\theta_{i,k}\right)|$. As a result, treating the NRFs and NPFs separately can be used for tackling difficult scenarios. We call the combination of NRF and NPF features a *Combined Distance of Normalized Polar Feature and Normalized Rectangular Feature* (CDPR). The reason why both NPF (7) and NRFs (9) are normalized in the same way is to avoid bias from different scales.

The following steps summarize the computation of feature distance between UE i and UE j using CDPR:

1) Calculate the distance of the NPF of UE i and UE j using (8).
2) Calculate the distance of the NRF of UE i and UE j as:

$$d^{i,j}_{\text{NRF}} = \min_{k,l} d\left(\mathbf{f}^{i,k}_{\text{NRF}}, \mathbf{f}^{j,l}_{\text{NRF}}\right),$$

where $d\left(\mathbf{f}^{i,k}_{\text{NRF}}, \mathbf{f}^{j,l}_{\text{NRF}}\right) = \|\mathbf{f}^{i,k}_{\text{NRF}} - \mathbf{f}^{j,l}_{\text{NRF}}\|_2$.

3) Compute the combined distance between UE i and UE j as:

$$d^{i,j}_{\text{CDPR}} = \min\left\{d^{i,j}_{\text{NPF}}, d^{i,j}_{\text{NRF}}\right\}. \tag{10}$$

V. Channel Charting

The underlying assumption of CC is that there exits a continuous mapping from the spatial location $\boldsymbol{z}_u$ of UE u to the CSI feature $\mathbf{y}_u$ at the BS [4]:

$$\mathcal{H} : \mathbb{R}^\rho \to \mathbb{C}^F; \quad \mathcal{H}(\boldsymbol{z}_u) = \mathbf{y}_u. \tag{11}$$

Here, ρ is the spatial dimension which is either 2 or 3, and F is the feature dimension. CC starts by measuring the distance

of the CSI features between pairs of UEs as seen at the BS. Next, based on the distance matrix, low dimensional channel chart is found in a *self-supervised manner*, providing chart locations for the set of UEs, such that UEs that are neighbors in the physical space will be neighbors in the channel chart. Several dimensionality techniques have been considered for CC. We apply t-Distributed Stochastic Neighbor Embedding (t-SNE) [19] for CC, as it has been shown to perform well in [16], [20].

VI. Performance Evaluation

To assess feature performance, we assume that the original space is the physical location space, and the representation space is the CSI feature space. Note that this differes from direct CC performance evaluation, where the representation space woudl be the low-dimensional channel chart. The distance in the original space is based on Euclidean distance, while the distance in the representation space is based on CSI feature distance.

To measure the degree of preserving the local topology, we consider the continuity (CT) and trustworthiness (TW). For a data set of U points, these can be computed by considering a neighborhood of J points, denoted as $V_J(\mathbf{z}_i)$, around locations $\{\mathbf{z}_i\}_{i=1}^{U}$ in the original space, and the J-neighborhood denoted as $V_J'(\mathbf{y}_i)$, around the corresponding points $\{\mathbf{y}_i\}_{i=1}^{U}$ in the representation space. The equations to compute the average values are given as [21]:

$$\mathrm{CT}(J) = 1 - a \sum_{i} \sum_{\substack{j \in V_J(\mathbf{z}_i) \\ j \notin V_J'(\mathbf{y}_i)}} \left(r(i,j) - J\right), \tag{12}$$

$$\mathrm{TW}(J) = 1 - a \sum_{i} \sum_{\substack{j \notin V_J(\mathbf{z}_i) \\ j \in V_J'(\mathbf{y}_i)}} \left(r'(i,j) - J\right), \tag{13}$$

where $r(i,j)$ is the rank of a point $\mathbf{z}_i$ in terms of its distance from a point $\mathbf{z}_j$ in original space, $r'(i,j)$ is the rank of a point $\mathbf{y}_i$ in terms of its distance from a point $\mathbf{y}_j$ in the representation space and $a = \frac{2}{UJ(2U-3J-1)}$ is a normalization factor.

Global geometry preservation is measured by the Kruskal Stress (KS). It is computed by comparing pairwise distance matrix $\bar{\mathbf{D}}$ of the points in original space $\{\mathbf{z}_i\}_{i=1}^{U}$ with pairwise distance matrix $\mathbf{D}$ of points in the representation space $\{\mathbf{y}_i\}_{i=1}^{U}$ using a distance scaling factor λ as [22]:

$$\mathrm{KS} = \min_{\lambda} \sqrt{\frac{\sum_{i,j} \left(d_{i,j} - \lambda \bar{d}_{i,j}\right)^2}{\sum_{i,j} d_{i,j}^2}}, \tag{14}$$

where $\bar{d}_{i,j} = \|\mathbf{z}_i - \mathbf{z}_j\|_2$ and $d_{i,j} = d(\mathbf{y}_i, \mathbf{y}_j)$.

All three metrics are in the range $[0,1]$ with the optimal value being 1 for TW and CT and 0 for KS.

VII. Simulations Results

A. Simulation Settings

We use the DeepMIMO data set to generate the CSI [23]. Channels are constructed based on ray-tracing data obtained from the Remcom Wireless InSite [24] channel emulator.

TABLE I
Simulation parameters.

Parameter	Value	Parameter	Value
Center Freq.	3.5 GHz	Subcarriers	4086
Scenario	O1-3p5	BW	100 MHz
BS Location	[287.5, 489.5] m	UE Locations	Vert. str.
BS Height	6	UE Height	2 m
BS Array	32 ULA	UE Array	1

Fig. 4. Simulation layout. The selected street segment is in pink colour. Two BSs are indicated by a red and blue stars.

Figure 4 shows the simulation layout. Two BSs are considered, marked with red and blue stars in the layout. The UEs are located in the southern part of the vertical street. The streets have buildings on both sides. Buildings are 60 m×60 m or 60 m×30 m, with the height written on the layout. A distance of 1.2 m between adjacent UEs samples is considered. Table I summarizes the simulation parameters. For the red BS, some locations in the street are blocked.

The data set consists of 4100 UE locations for the red marked BS, after filtering out the blocked locations. The set for the the blue marked BS consists of 4400 UE locations. The super-resolution features are taken directly from the data set. As seen from the simulation layout in Figure 4, BS4 (red star) and at BS6 (blue star) represents NLoS scenario and LoS scenario, respectively.

B. CSI Feature and Distance Evaluation

We consider the following benchmark features and distances:

- The MPS feature as in (4) with Euclidean distance to compute the pairwise distance between MPCs of two UEs [15]. Then the minimum pairwise distance is used to measure the distance between the two UEs.
- The APF given as in (5) with Euclidean distance to compute the pairwise distance between MPCs of two UEs.

TABLE II
PERFORMANCE MEASURES FOR DIFFERENT CSI FEATURES AND DISTANCES IN EXAMPLE 1. ALL MEASURES ARE IN $[0, 1]$; ↑ LARGE IS BETTER; ↓ SMALL IS BETTER.

CSI Feature + Dist.	CT↑	TW↑	KS↓
MPS + Euc.	0.642	0.855	0.831
APF + Euc.	0.933	0.955	0.952
SRF + EMD	0.995	0.976	0.266
SRF + Euc.	0.999	0.989	0.294
NRF + Euc.	**0.999**	0.989	0.289
NPF + Euc.	0.997	**0.999**	0.198
CDPR	0.997	**0.999**	**0.197**

TABLE III
PERFORMANCE MEASURES FOR DIFFERENT CSI FEATURES AND DISTANCES IN EXAMPLE 2. ALL MEASURES ARE IN $[0, 1]$; ↑ LARGE IS BETTER; ↓ SMALL IS BETTER.

CSI Feat + Dist.	CT↑	TW↑	KS↓
MPS + Euc.	0.724	0.844	0.722
APF + Euc.	0.836	0.991	0.233
SRF + EMD	0.996	0.992	0.148
SRF + Euc.	0.999	0.999	0.015
NRF + Euc.	0.999	0.999	**0.014**
NPF + Euc.	0.999	0.999	0.041
CDPR	0.999	0.999	0.027

Then the minimum pairwise distance is used to measure the distance between the two UEs.
- The SRF given in (6) with EMD to compute the distance between two sets of MPCs as in [11].
- The SRF given in (6) with Euclidean distance to compute the pairwise distance between MPCs of two UEs. Then the minimum pairwise distance is used to measure the distance between the two UEs.

We examine the performance of the following proposed features and distances:

- The NPF given in (7) with the with Euclidean distance to compute the pairwise distance between MPCs of two UEs. Then the minimum pairwise distance is used to measure the distance between the two UEs.
- NRF in (9) with the with Euclidean distance to compute the pairwise distance between MPCs of two UEs. Then the minimum pairwise distance is used to measure the distance between the two UEs.
- CDPR using the NPF and NRF and applying (10) to compute the distance between two UEs.

C. Example 1: Challenging NLoS Scenario

The CSI of the UEs seen at red marked BS (BS 4 in DeepMIMO) in the layout in Figure 4 is considered. The majority of UE locations have NLoS propagation. We evaluate the performance of several CSI features and distances in terms of CT, TW and KS. We consider $J = 100$ neighbours (which corresponds to 2.4% of the data set) to compute the CT and TW. The results are presented in Table II.

As seen from Table II, the proposed CDPR gives state-of-the art feature performance as compared to the CSI features and distances from the literature in this example.

D. Example 2: LoS Scenario

The CSI of the UEs seen at blue marked BS (BS 6 in DeepMIMO) in the layout in Figure 4 is considered. The majority of UE locations have LoS propagation.

The CSI feature and distance performance results of this scenario are presented in Table III. As seen from the table, the best performance is obtained by the proposed NRF+Euc, which is very close to the performances of the SFR+Euc and the proposed CDPR.

E. Channel Charting Results

We consider the t-Distributed Stochastic Neighbor Embedding (t-SNE) to create the channel chart. The perplexity parameters is tuned to give the best results in terms of the TW, CT and KS performance results. The channel charts for Example 1 and Example 2 are shown in Figure 5 and Figure 6, respectively. We create the channel chart for SRF with EMD and the combined distance CDPR. The figures show that CC based on CDPR looks much better for both LoS and NLoS scenarios compared to the SRF with EMD.

VIII. CONCLUSIONS

In this paper we considered angle-delay super resolution Channel State Information (CSI) feature for Channel charting. In challenging None-Line-of-Sight (NLoS) propagation conditions, the received signal at the base station from two nearby locations may have a small angle difference but a large delay difference. Considering the Cartesian coordinate (rectangular) CSI feature representation may lead to a large CSI distance. To tackle this problem, we treated the angle and delay separately and formulated the normalized polar CSI feature. We considered the Euclidean distance to measure the distance between two multi-path components, each belonging to a different User Equipment (UE). We consider the minimum pair-wise distance to measure the distance between two UEs. To handle different propagation conditions, we combined the distances in the normalized rectangular feature space and the normalized polar feature space. Simulation results based on the DeepMIMO data-set show that the proposed super-resolution representation with the Euclidean distance provides state-of-the-art CC quality.

ACKNOWLEDGMENT

This work was supported by the CHIST-ERA project CHASER, through Research Council of Finland grant 359837.

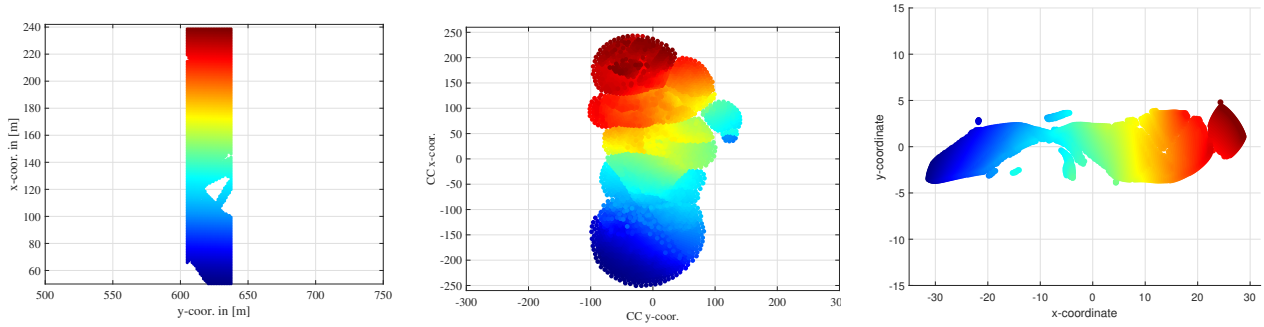

Fig. 5. Example 1: red marked BS: (Left): UE physical location, sampled UE locations marked by colors. (Middle): CC based on EMD. (Right): CC based on CDPR. CC locations are marked by colors corresponding to the physical locations.

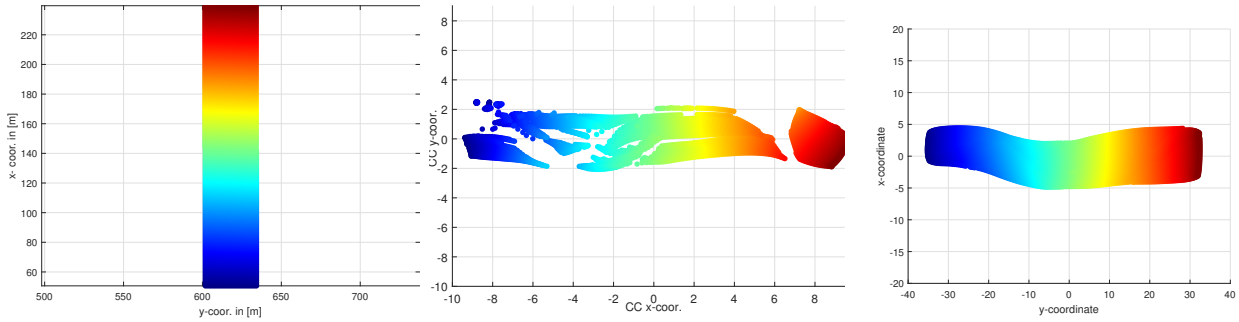

Fig. 6. Example 2 : (Left): UE physical location, sampled UE locations marked by colors. (Middle): CC based on EMD. (Right) CC based on CDPR. CC locations are marked by colors corresponding to the physical locations.

REFERENCES

[1] S. Dwivedi, R. Shreevastav, F. Munier, J. Nygren, I. Siomina, Y. Lyazidi, D. Shrestha, G. Lindmark, P. Ernström, E. Stare, S. M. Razavi, S. Muruganathan, G. Masini, Å. Busin, and F. Gunnarsson, "Positioning in 5G networks," *IEEE Commun. Mag.*, vol. 59, no. 11, pp. 38–44, 2021.

[2] X. Fang, W. Feng, Y. Chen, N. Ge, and Y. Zhang, "Joint communication and sensing toward 6G: Models and potential of using MIMO," *IEEE Internet Things J.*, vol. 10, no. 5, pp. 4093–4116, 2023.

[3] A. Xhafa, J. A. del Peral-Rosado, J. A. Lopez-Salcedo, and G. Seco-Granados, "Evaluation of 5G positioning performance based on UTDoA, AoA and base-station selective exclusion," *Sensors*, vol. 22, no. 1, 2022.

[4] C. Studer, S. Medjkouh, E. Gonultas, T. Goldstein, and O. Tirkkonen, "Channel charting: Locating users within the radio environment using channel state information," *IEEE Access*, vol. 6, pp. 47 682–47 698, 2018.

[5] L. Maaten, E. Postma, and H. Herik, "Dimensionality reduction: A comparative review," 2008.

[6] L. L. Magoarou, "Efficient channel charting via phase-insensitive distance computation," *IEEE Wireless Commun. Lett.*, vol. 10, no. 12, pp. 2634–2638, 2021.

[7] P. Kazemi, H. Al-Tous, T. Ponnada, C. Studer, and O. Tirkkonen, "Beam SNR prediction using channel charting," *IEEE Trans. Veh. Technol.*, pp. 1–16, 2023.

[8] P. Ferrand, A. Decurninge, L. G. Ordonez, and M. Guillaud, "Triplet-based wireless channel charting: Architecture and experiments," *IEEE J. Sel. Areas Commun.*, vol. 39, no. 8, pp. 2361–2373, 2021.

[9] C.-X. Wang, J. Bian, J. Sun, W. Zhang, and M. Zhang, "A survey of 5g channel measurements and models," *IEEE Communications Surveys & Tutorials*, vol. 20, no. 4, pp. 3142–3168, 2018.

[10] H. Xu, Y. Zhang, B. Ba, D. Wang, and X. Li, "Fast joint estimation of time of arrival and angle of arrival in complex multipath environment using OFDM," *IEEE Access*, vol. 6, pp. 60 613–60 621, 2018.

[11] H. AL-Tous, P. Kazemi, C. Studer, and O. Tirkkonen, "Channel charting with angle-delay-power-profile features and earth-mover distance," in *Proc. of Asilomar Conference on Signals, Systems, and Computers*, 2022, pp. 1195–1201.

[12] A. Sobehy, E. Renault, and P. Muhlethaler, "CSI-MIMO: K-nearest neighbor applied to indoor localization," in *Proc. ICC*, 2020, pp. 1–6.

[13] X. Sun, X. Gao, G. Y. Li, and W. Han, "Single-site localization based on a new type of fingerprint for massive MIMO-OFDM systems," *IEEE Trans. Veh. Technol.*, vol. 67, no. 7, pp. 6134–6145, 2018.

[14] E. Gonultas, E. Lei, J. Langerman, H. Huang, and C. Studer, "CSI-Based multi-antenna and multi-point indoor positioning using probability fusion," *IEEE Trans. Wireless Commun.*, vol. 21, no. 4, pp. 2162–2176, 2022.

[15] B. Fleury, M. Tschudin, R. Heddergott, D. Dahlhaus, and K. I. Pedersen, "Channel parameter estimation in mobile radio environments using the SAGE algorithm," *IEEE J. Sel. Areas Commun.*, vol. 17, no. 3, pp. 434–450, 1999.

[16] J. Deng, S. Medjkouh, N. Malm, O. Tirkkonen, and C. Studer, "Multipoint channel charting for wireless networks," in *Proc. Asilomar Conf. Sign., Syst., Comput.*, Oct. 2018, pp. 286–290.

[17] N. Czink, P. Cera, J. Salo, E. Bonek, J. pekka Nuutinen, and J. Ylitalo, "A framework for automatic clustering of parametric MIMO channel data including path powers," in *Proc. of IEEE VTC*, 2006, pp. 1–5.

[18] M. Steinbauer et.all, "How to quantify multipath separation," *IEEE Trans. Electron*, vol. E82, pp. 1–5, 1999.

[19] L. van der Maaten and G. Hinton, "Visualizing data using tSNE," *J Mach Learn Res*, vol. 9, pp. 2579–2605, Nov. 2008.

[20] L. van der Maaten, "Learning a parametric embedding by preserving local structure," in *AISTATS*, 2009.

[21] J. Venna and S. Kaski, "Neighborhood preservation in nonlinear projection methods: An experimental study," in *Proc. ICANN*, 2001, pp. 485–491.

[22] J. B. Kruskal, "Multidimensional scaling by optimizing goodness of fit to a nonmetric hypothesis," *Psychometrika*, vol. 29, pp. 1–27, 1964.

[23] A. Alkhateeb, "DeepMIMO: A generic deep learning dataset for millimeter wave and massive MIMO applications," in *Proc. ITA*, Feb. 2019, pp. 1–8.

[24] Remcom, "Wireless InSite," http://www.remcom.com/wireless-insite.